

Article

Analysis and Experiments on the Characteristics of Airflow and the Air Cleanliness Protection Region under Fan Filter Units in Cleanrooms

Hao Li , Chen Huang, Weiqi Yi and Chao Li

School of Environment and Architecture, University of Shanghai for Science and Technology, Shanghai 200093, China; hcyhywj@163.com (C.H.); yiweiqi1998@163.com (W.Y.); leecc3161@163.com (C.L.)

* Correspondence: lihao@usst.edu.cn

Abstract: Cleanrooms often utilize large amounts of supply air to achieve a required cleanliness level. To reduce the overall supply air volume, critical processes demanding the highest cleanliness requirements are suggested to be placed directly beneath the air outlet of fan filter units (FFUs). In order to determine an appropriate supply air volume, it is necessary to quantitatively analyze the particulate concentration distribution downstream of FFUs with various characteristics to determine an adequate but not excessive supply air volume. Three FFU sizes and four supply air velocities were used in this experiment, and the resulting airstream velocities, jet diffusion widths, and characteristics of particulate concentration distribution were obtained. Fitting expressions were statistically acquired based on the respective experimental data sets, which can be used to predict the airflow velocity value at any point in an FFU flow region and the width of the air cleanliness protection range.

Keywords: airflow field of FFU; particulate concentration distribution; air cleanliness protection range



check for updates

Citation: Li, H.; Huang, C.; Yi, W.; Li, C. Analysis and Experiments on the Characteristics of Airflow and the Air Cleanliness Protection Region under Fan Filter Units in Cleanrooms. *Sustainability* **2023**, *15*, 13268. <https://doi.org/10.3390/su151713268>

Academic Editor: Ying Sheng

Received: 14 July 2023

Revised: 24 August 2023

Accepted: 1 September 2023

Published: 4 September 2023



Copyright: © 2023 by the authors. Licensee MDPI, Basel, Switzerland. This article is an open access article distributed under the terms and conditions of the Creative Commons Attribution (CC BY) license (<https://creativecommons.org/licenses/by/4.0/>).

1. Introduction

Cleanroom spaces are widely used in semiconductor production, pharmaceutical manufacturing, medical surgery rooms, etc., where environmental conditions, especially particulate concentration, are controlled within specified limits [1,2]. Unlike in office spaces, much higher airflow intensity using many high-efficiency particulate air filters (HEPA) is often necessary in cleanrooms to reduce indoor particulate concentration in order to enhance air cleanliness. This high flow intensity requirement, which could be 30~50 times higher than that of commercial buildings, leads to substantially high energy consumption in air-conditioning systems [3–6].

Many researchers have conducted studies from different perspectives to reduce energy consumption and maintain cleanliness requirements of cleanrooms. Some early researchers focused on the average cleanliness (average concentration value) in cleanrooms: they used the particle count conservation equation to establish the relationship between indoor particle emission/generation levels, supply air volume, filtration efficiency, indoor particulate concentration, etc. [7–11]. For example, W. Whyte et al. established some equations to calculate the particulate concentration and microbe-carrying particles in non-unidirectional airflow cleanrooms [7]. L. Zhou et al. analyzed five well-recognized mathematical models for calculating the particulate concentration in cleanrooms and compared their calculation results with experiments [8]. W. Sun et al. used a principle to estimate the required air flow rate based on actual conditions and cleanliness requirements of a cleanroom instead of selecting an arbitrary value based on opinion or estimating from a wide range of flow rates [9]. Although the equations and models based on particle count conservation are widely used, the particulate concentration in cleanrooms is non-uniform and varies significantly at different locations [12]. The main factors that could influence the particulate distribution in a cleanroom are the particle emission/generation level, layout and size

of supply air outlets and return air grilles, size and shape of the room, behavior of staff, etc. Therefore, even if the calculated supply air volume is used based on the principle of particle count conservation, the local cleanliness in cleanrooms can vary significantly above or below the room-averaged value.

In recent years, some researchers studied the thermal environment and particulate concentration distribution in cleanrooms using CFD simulation and experiments to determine the appropriate supply air volume [13–18]. W Whyte et al. compared the airflow distribution and particulate concentration in a four-way diffuser with a supply air outlet with no diffuser in a non-unidirectional flow cleanroom using CFD simulation and experiments. It was found that the four-way diffuser provided much better air mixing and a more even particle concentration throughout the cleanroom, while a HEPA unit with no diffuser provided a pronounced downward jet flow and low levels of particulate concentration below it [13]. M. Loomans et al. found that controlling the supply air volume based on the number of people indoors was the most energy-saving strategy for pharmaceutical cleanrooms. They also found that under various air distribution forms, the area that needed to be cleaned could be placed close to the supply air outlet where the highest cleanliness level could be obtained [14]. J. Zhao et al. used CFD simulation to calculate the accessibility index and describe the impact of particle sources on clean zones with various supply air volumes of FFUs, and then they calculated the required clean air volume in a non-unidirectional flow cleanroom [15]. These research results indicate that there are many factors affecting the particle distribution in cleanrooms and that the areas closer to the supply air outlet have higher air cleanliness. Obviously, the region directly under a supply air outlet can obtain the highest air cleanliness level. Therefore, critical processes or operations demanding the highest cleanliness requirements can be placed directly beneath an air outlet, while non-critical operations can be placed outside this region. This disparate treatment of supply airflow intensity for critical and non-critical areas can significantly decrease the overall fan energy consumption in a cleanroom.

It is necessary to quantitatively analyze the characteristics of airflow and particulate concentration distribution downstream of supply air outlets with various supply air face velocities. However, prior studies on this topic are limited. In this paper, the airstream velocities and particulate concentration distributions under a supply air outlet in both the axial and radial directions (at cross section) in array positions were measured, and the relationships among the air velocity, particulate concentration distribution, and different influencing factors were further investigated.

2. Experimental Setup

2.1. Estimated FFU Airflow Pattern

In this study, a fan filter unit (FFU) was used as the supply air outlet. Figure 1 shows the estimated airflow pattern of supply air from an FFU based on a turbulent jet system [19–24]. The half-width of the FFU face surface is denoted by R_0 . The FFU face velocity and particulate concentration of the discharged air are denoted by u_0 and c_0 , respectively. x represents the axial (vertical) distance from the FFU, and y represents the radial (horizontal) distance at the cross-section from the vertical axis.

The high-speed air jet from the FFU plunges forcefully into the surrounding air and creates turbulence. The jet flow can be divided into two distinct regions in the axial direction: the flow development region and the fully developed flow region [19,20]. According to ASHRAE's suggestion [25], the boundary between the two regions is $x = (0.57\sim 1.48) \times (R_0)^{0.5}$. Although cleanroom height varies widely in application, 3 m is a common height. The typical height of a workspace ranges from 0.8 m to 1.5 m from the floor; therefore, the distance between a workspace and a supply air outlet is about 1.5~2.2 m. The face dimension of a typical FFU is 0.61 m \times 0.61 m; thus, its half-width is 0.305 m. It can be calculated that the length of a flow development region from a supply air outlet is less than 0.8 m. Therefore, a workspace is generally in the fully developed flow region, and this study is mainly aimed at this region.

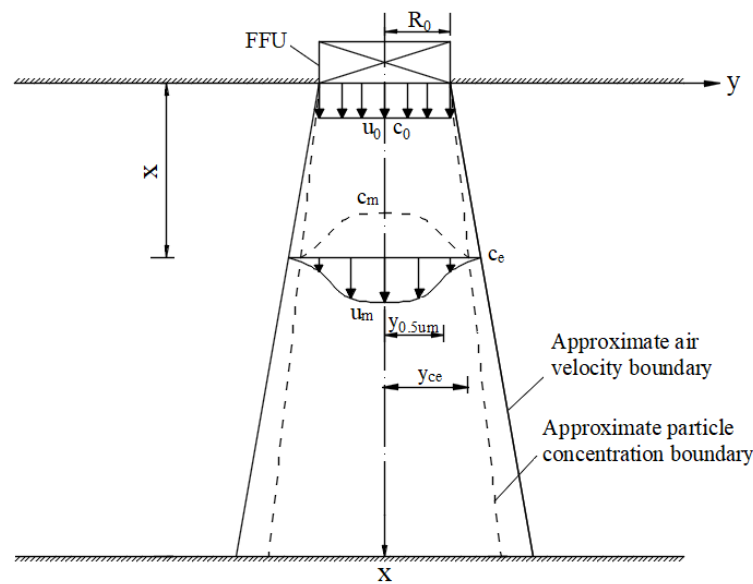


Figure 1. Supply airflow pattern under an FFU.

In the fully developed flow region, u_m and c_m are the airstream velocity and particulate concentration, respectively, on the x -axis. The particulate concentration in the surrounding environment is given by c_e . The solid lines in Figure 1 represent the estimated velocity boundary from the FFU jet airstream, where the velocity approaches zero. $y_{0.5um}$ represents the lateral distance y where the velocity is 50% of the u_m . Similarly, represents the lateral distance y where the particulate concentration is equal to the ambient particulate concentration c_e , and the dotted lines indicate the estimated particulate concentration boundary.

2.2. Experimental Cleanroom and Measurement Points

In this study, the experimental cleanroom has a length of 4.445 m, a width of 3.2 m, and a height of 2.1 m, as shown in Figure 2. The cleanroom is equipped with 14 FFUs, each having a HEPA media (H14 filter class, 99.997% efficiency for particles $\geq 0.3 \mu\text{m}$). Because the height of the experimental cleanroom is less than 3 m, an FFU with dimensions $0.38 \text{ m} \times 0.38 \text{ m}$ is selected as the experimental object. This may result in a relatively short length of the flow development region from the FFU, about 0.25–0.65 m, while the region about 1.45 m to 1.85 m above the floor is in a fully developed region.

The layout of the experimental setup in the cleanroom is shown in Figure 2a. The selected FFU installed at the ceiling, shown as the dashed rectangle in Figure 2b, has a motor speed control system. The supply air velocity of the FFU is adjustable from 0.1 to 1.5 m/s. On each of the two sidewalls, there are three return air grilles, each with dimensions $0.5 \text{ m} \times 0.3 \text{ m}$. The combined surface area of the return grilles is 0.9 m^2 ($2 \times 3 \times 0.5 \text{ m} \times 0.3 \text{ m}$). The height from the floor to the bottom of the grilles is 0.1 m. The airflow pattern starts from the ceiling FFU toward the sidewall return air grilles as the primary airstream passage.

Indoor particle emissions can be generated using an external (remote) aerosol generator placed outside the cleanroom. The aerosol generator uses clean compressed air to nebulize a DI water solution, which contains many polystyrene microspheres (PSL) of a desired particle size. The aerosol can be remotely delivered from the generator through a 1 m long, 0.02 m diameter rigid tubing rod into the cleanroom. In this study, the rod was vertically installed between 0.8 m and 1.8 m above the floor and 1.5 m from the axis of the FFU. To stabilize the particulate concentration in the surrounding environment, four holes with a diameter of 4 mm were opened on the reverse side of the rod relative to the supply air region, with a uniform spacing of 0.3 m between the holes. Aerosol particles were released from these holes into the cleanroom. An aerosol particle diameter of $0.5 \mu\text{m}$ was used for the in-room emission and particle sensing in this study. The emission was assumed to come from two persons. The emission rate was about 10^5 particles/(min·person).

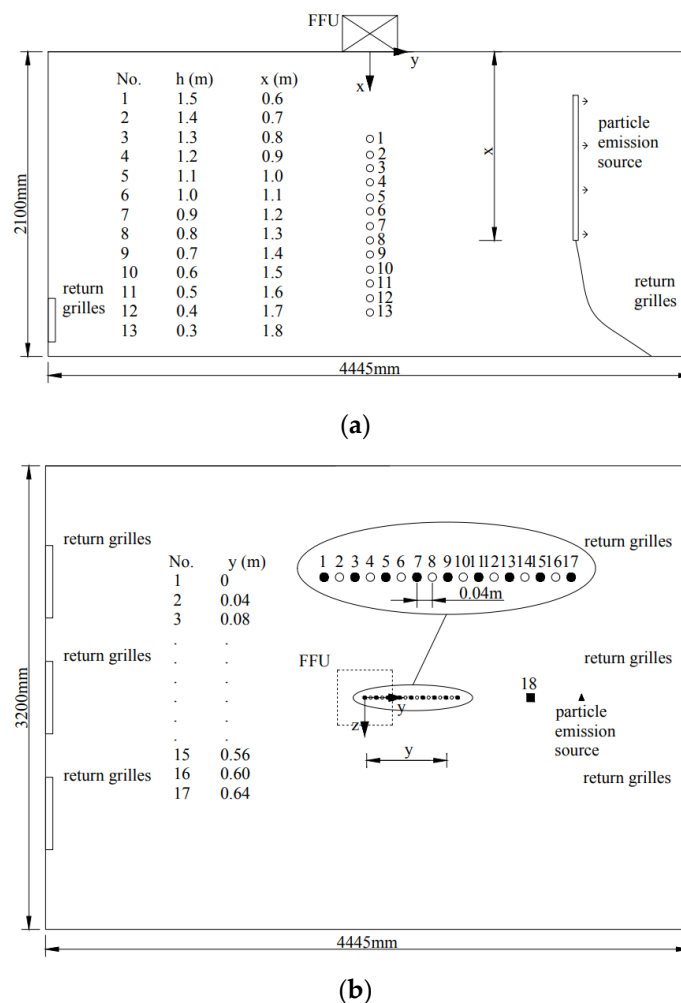


Figure 2. Schematic diagram showing the distribution of experimental measurement points. (a) Vertical section and (b) horizontal section.

A schematic diagram showing the measurement point setup is provided in Figure 2. The air velocity measurement points in the supply air path (axial direction) were located between 0.6 and 1.8 m from the FFU with a uniform spacing of 0.1 m between points (the points numbered 1 to 13 in Figure 2a). In the horizontal direction (radial direction at the cross-section), 16 points (the points numbered 1 to 16 in Figure 2b) were arranged at a lateral distance of 0~0.6 m from the axis of the FFU with a uniform spacing of 0.04 m between points.

The measurement points of particulate concentration were located at three heights, i.e., 0.8 m, 1.0 m, and 1.2 m from the floor (the horizontal plane where measurement points 4, 6, and 8 in Figure 2a). There were nine measured points in the horizontal direction, located between 0 and 0.64 m from the axis of the FFU (the black solid points numbered 1, 3, 5...17 in Figure 2b), with a uniform spacing of 0.08 m between points. Point 18 in Figure 2b is the measurement point (1.15 m from the axial centerline of FFU) for measuring the particulate concentration of the surrounding zone.

2.3. Instruments and Experimental Conditions

An airborne particle counter (Lighthouse handheld 3016-IAQ) was used to measure the particulate concentration at different positions in the experiments. The particle sizes measured were between 0.3 and 25.0 μm , and the flow rate was 0.1CFM (2.83LPM). The counting efficiency was 100% for particles > 0.45 μm . An ultrasonic anemometer (Sonic Corporation, Model WA-790) was used to sense air velocities along both the axial and

radial directions, in a range of 0~10 m/s with an accuracy of +2% and resolution of ± 0.02 m/s. A thermal anemometer (Testo 425) was used for the FFU face velocities, in a range of 0~20 m/s with an accuracy of ± 0.03 m/s (+5% of mv).

Table 1 shows the average face velocity of the FFU, supply air volume, and Reynolds number under four experimental conditions. The size and face velocity of supply air from the FFU are the most important factors. Considering that the experimental FFU and a typical FFU are different in size, the Reynolds number is calculated to ensure that the motion is similar. The typical FFU size is $0.61 \text{ m} \times 0.61 \text{ m}$, and the face velocity is generally 0.3~0.45 m/s; thus, the Reynolds number is 11,656~17,548. In this study, the experimental FFU size was $0.38 \text{ m} \times 0.38 \text{ m}$, and the Reynolds number for the four experimental conditions was 6801~17,330, which covered typical FFU operating conditions.

Table 1. Experimental conditions.

Parameter	Unit	Case 1	Case 2	Case 3	Case 4
Average face velocity	m/s	0.281	0.362	0.467	0.716
Supply air volume	m ³ /h	146	188	243	372
Reynolds number	-	6801	8761	11,303	17,330

To ensure the stability and validity of these readings, after the FFU ran for 15 min, three replications of measurements were obtained at each measurement point for 60 s, and the averaged value of the three rounds was calculated as the shown result.

The walls and floor of the cleanroom were manually cleaned at the start and end of each measurement to ensure that the test room background did not contain residual particles that could cause a bias in the following test results.

3. Results

3.1. Variation in Air Velocity along the Axial Direction

In Figure 3 and the remaining discussions, a relative airflow velocity (normalized with the FFU discharge velocity) expressed in dimensionless form is used. Figure 3 shows the dimensionless air velocity along the FFU axial flow direction. It can be found that the velocity decreases gradually when the relative axial distance x/R_0 (normalized with the FFU half-width, dimensionless) exceeds 3.16 (about 0.6 m from the supply air outlet), except for the Case 1 condition, which cannot be accurately measured due to its low velocity. This indicates that the supply air jet is in a fully developed region beyond this distance, and the result meets the boundary between two distinct regions estimated above. The velocity attenuation trend is similar to various supply air velocities, and the velocity is inversely proportional to the distance from the FFU. In addition, the measured data for $x/R_0 > 8$ are significantly dispersed, owing to the close proximity to the floor.

For the axial velocity distribution of air jets, Rajaratnam [20] and Abramovich [19] conducted experimental and theoretical studies on circular and plane high-speed nozzle jets and derived corresponding empirical expressions. Rajaratnam's expression summarized the experimental results from multiple researchers, and Abramovich's semi-empirical expressions were obtained by combining the experimental results and the momentum conservation principle. The ASHRAE [25] analyzed various types of common supply air outlets and provided a general empirical expression for the axial velocity distribution. The results calculated using the expressions by Rajaratnam, ASHRAE, and Abramovich are shown in Figure 3. These expressions use the same empirical structure, but there are differences in the throw constants and exponents. Fitting for the same empirical structure from the measured data, a new dimensionless velocity profile expression for axial direction is obtained as follows:

$$\frac{u_m(x)}{u_0} = 1.422 \left(\frac{x}{R_0} \right)^{-0.338} \quad (1)$$

where $u_m(x)$ is the local velocity at the vertical distance x from the FFU.

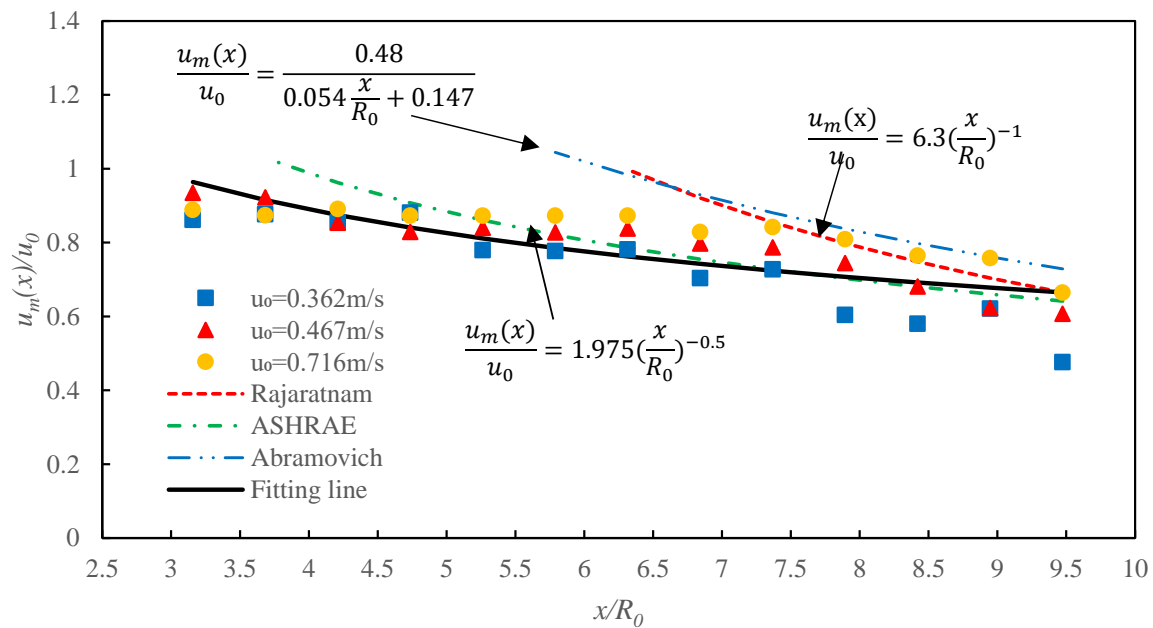


Figure 3. Dimensionless air velocity profile along the axial direction.

The new empirical curve calculated using expression (1) has the flattest slope compared with those of the existing curves. Rajaratnam's and Abramovich's curves were calculated only at higher velocities, which did not cover a broader discharge velocity range that is typical of FFUs; missing the lower velocity range leads to the exclusion of a milder entrainment of surrounding air and slower attenuation. Furthermore, Rajaratnam's and Abramovich's studies used circular nozzles, while this research used a rectangular face FFU, which is more common in cleanrooms. Although the ASHRAE expression was not intended for specific cleanroom applications, it is closer to the newly fitted curve, while Rajaratnam's and Abramovich's expressions may be less applicable for predicting axial velocity near the FFU discharge vicinity. Table 2 lists the mean absolute percentage errors (MAPEs) for these four expressions against the FFU-measured data.

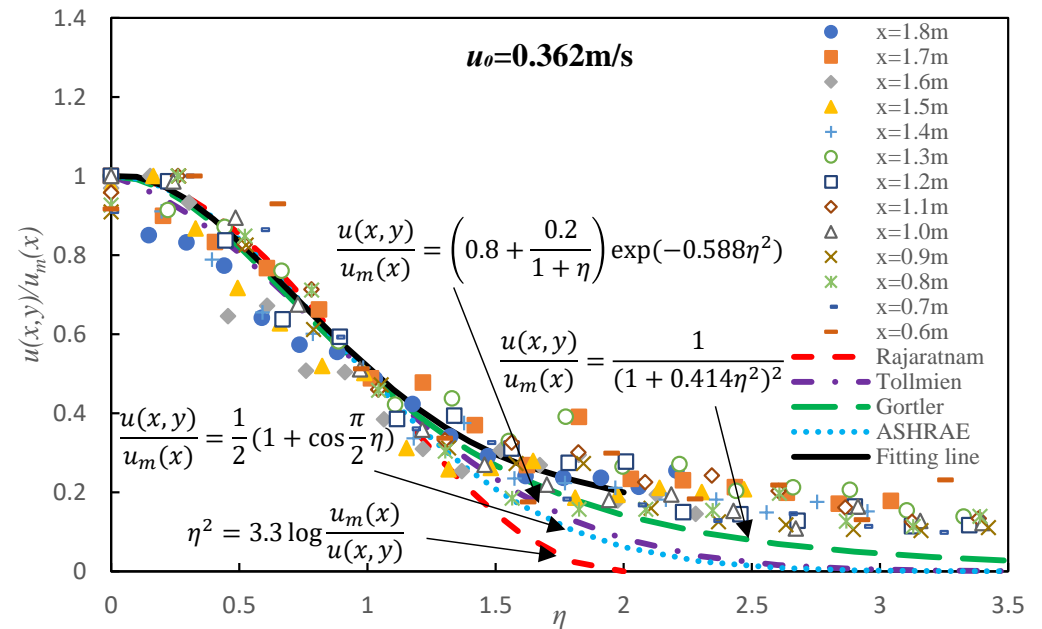
Table 2. MAPE values of air velocity along the axial direction for the existing expressions and fitted expression (1).

Test Case	Rajaratnam	Abramovich	ASHRAE	Fitted Expression (1)
$u_0 = 0.362$ m/s	23.7%	27.3%	11.1%	9.4%
$u_0 = 0.467$ m/s	13.5%	16.6%	5.9%	5.0%
$u_0 = 0.716$ m/s	9.3%	10.4%	9.2%	8.1%
Average	15.5%	18.1%	8.7%	7.5%

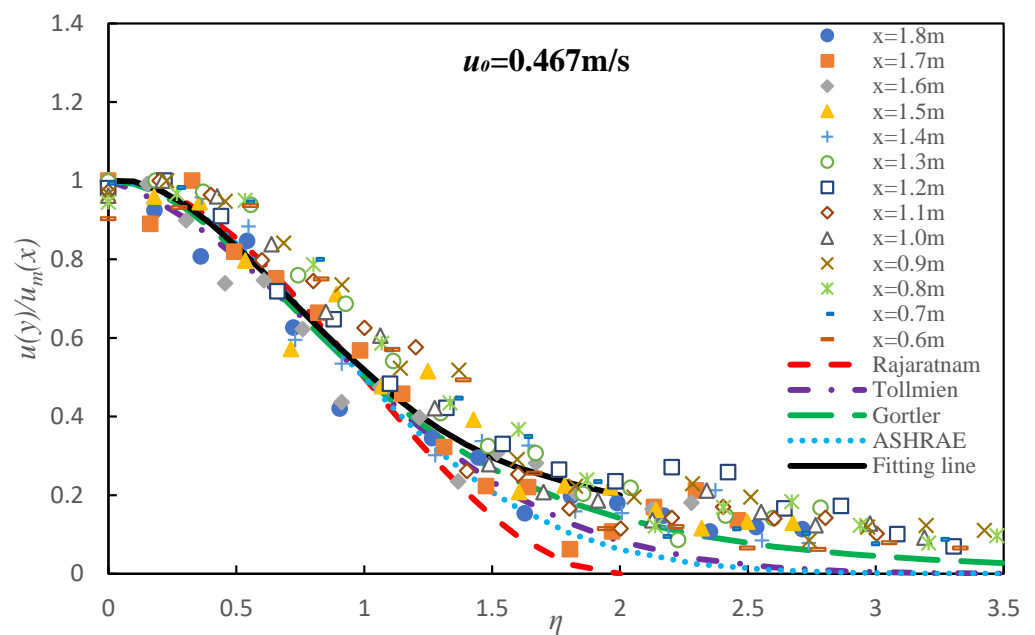
3.2. Lateral Air Velocity Distribution at Cross Sections

The dissipation of supply air entrains the surrounding room air, resulting in a gradual reduction in velocity and the formation of a mixed airstream. Velocity profiles were obtained with several FFU discharge velocities at various heights of cross-sections, as shown in Figure 4, where $u(x,y)$ denotes the local velocity at an axial/centerline distance x downstream of the FFU and a lateral distance y from the FFU centerline. Dimensionless velocity $u(x,y)/u_m(x)$ and dimensionless lateral distance η (noted as $y/y_{0.5u_m}$) are used in Figure 4 to represent the vertical and horizontal axes, respectively. In most studies, it is difficult to measure the jet radial boundary width accurately, and the fractional distance method is usually used, that is, the diffusion width is defined by the lateral distance y where the air velocity u drops at 50% of the FFU face velocity u_m in a half (one-side) width $y_{0.5u_m}$ [24,26–28]. The velocity $u(x,y)/u_m(x)$ decreases with the increase in lateral distance η .

With the increase in FFU face velocity, the velocity profiles gradually become self-similar. It is clear that a higher face velocity creates a stronger diffusion against the interference of surrounding air in the room.



(a)



(b)

Figure 4. Cont.

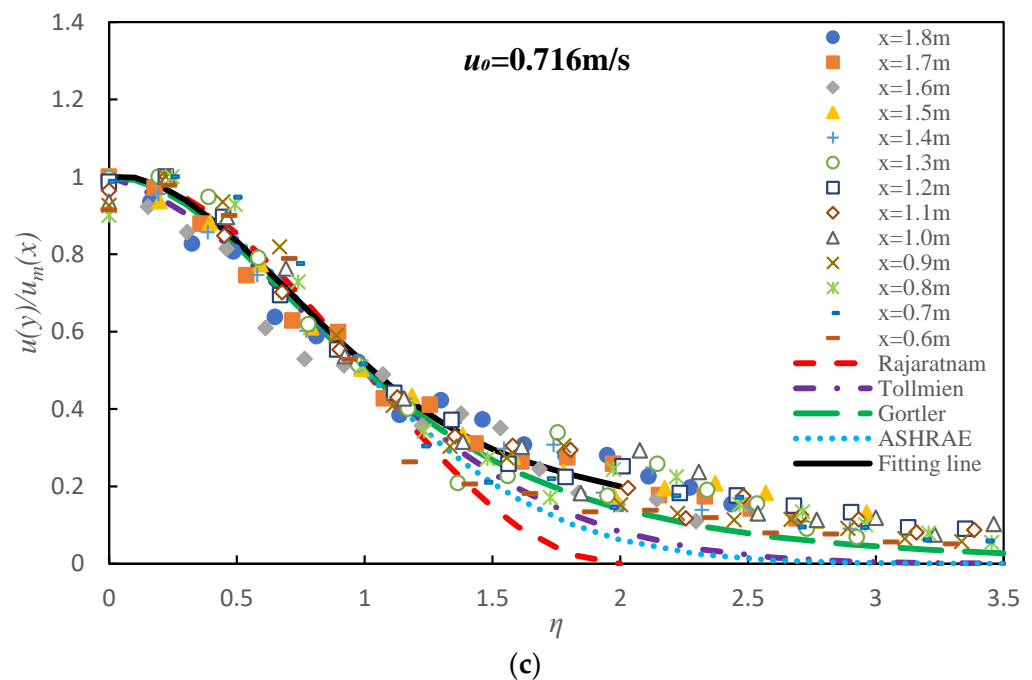


Figure 4. Downstream air velocity profiles along the lateral distance under three FFU discharge velocities: (a) $u_0 = 0.362$ m/s; (b) $u_0 = 0.467$ m; and (c) $u_0 = 0.467$ m.

Figure 4 shows four existing expressions (either theoretically or empirically based) and their curves by Rajaratnam [20], Tollmien [29], Gortler [30], and ASHRAE [25]. In comparison with the lab-measured data, when the lateral distance η is < 1 , the velocities $u(x,y)/u_m(x)$ predicted using the four expressions are in good agreement with the experimental data. When $\eta > 1$, these predicted velocities are higher than the experimental values. This implies that the measured lateral diffusion range of the FFU is much wider than the predictions calculated using the existing expressions. In order to generate a more comprehensive expression specifically for cleanroom applications that covers a broader FFU discharge velocity range (the three tested velocities) that also is based on the stringently controlled cleanroom test conditions, a new expression for the FFU air velocity profile along the lateral distance is developed, as shown in expression (2). Table 3 lists the MAPE values for the four existing expressions and the new expression (2).

$$\frac{u(x,y)}{u_m(x)} = -0.1472\eta^4 + 0.7714\eta^3 - 1.2003\eta^2 + 0.0925\eta + 1 \quad (2)$$

Table 3. MAPE values of air velocity along the lateral distance for the existing expressions and the fitted expression (2).

Test Case	Rajaratnam	ASHRAE	Tollmien	Gortler	Fitted Expression (2)
$u_0 = 0.362$ m/s	27.3%	18.4%	16.0%	12.2%	11.7%
$u_0 = 0.467$ m/s	30.7%	21.5%	19.2%	15.4%	14.8%
$u_0 = 0.716$ m/s	26.9%	24.2%	15.1%	10.7%	11.3%
Average	28.3%	21.4%	16.7%	12.8%	12.6%

3.3. Width of Air Velocity Diffusion

This study used the definition of airflow velocity diffusion width (boundary) as the lateral distance (or called half width) at which the axial velocity of the air jet reaches 50% of the FFU discharge (face) velocity. It provides a measure of how the airflow spreads as it moves away from the FFU outlet. The full width of the diffusion is the doubled lateral distance, which encompasses the entire spread of two symmetrical sides. Figure 5 shows

the curves for the dimensionless diffusion width $y_{0.5um}/R_0$ at various cross sections using two existing empirical models by Yin [19] and Rajaratnam [15]. Both models show that the diffusion width $y_{0.5um}/R_0$ increases linearly with the increase in axial distance x/R_0 and is independent of the supply air face velocity. A better-fitted expression was therefore developed and expressed as follows:

$$\frac{y_{0.5um}}{R_0} = 0.0961 \left(\frac{x}{R_0} + 4.4537 \right) \quad (3)$$

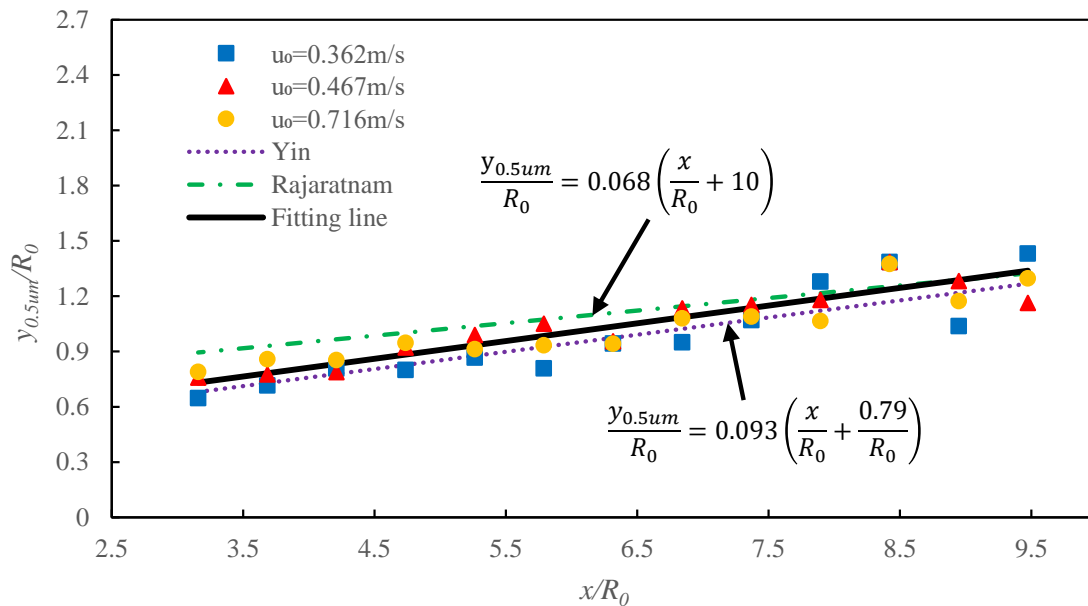


Figure 5. Relationship between the diffusion width $y_{0.5um}/R_0$ and lateral distance x/R_0 .

The spread rate obtained in this study is 0.0961, which is very close to the speed rate (0.093) in Yin's model that used an air curtain jet pattern, but it is different from the speed rate (0.068) in Rajaratnam's model. A possible reason is that this experiment and Yin's study used vertical downward discharge from the ceiling, while Rajaratnam's model was based on the side-wall jet pattern. A higher spread rate also indicates that the airflow from the FFU has a larger diffusion range, and its width increases faster than those using diffuser types of air outlets that are commonly used for commercial spaces. Table 4 lists the MAPE values for Yin's and Rajaratnam's empirical expressions and the experimental results.

Table 4. MAPE values of diffusion width vs. lateral distance for the existing expressions and the fitted expression (3).

Test Case	Rajaratnam	Yin	Fitted Expression (3)
$u_0 = 0.362$ m/s	20.0%	7.5%	11.1%
$u_0 = 0.467$ m/s	9.4%	8.0%	5.2%
$u_0 = 0.716$ m/s	10.5%	7.0%	6.3%
Average	13.3%	7.5%	7.6%

3.4. Spread of FFU Clean Air along the Axial Direction

The discharge of FFU air into a room can create a clean air protection zone under the FFU and form a cone-shaped clean air boundary along the axial direction, as shown in Figure 1. Along the axial and lateral directions, this effect of clean air gradually disappears when the clean airstream particle concentration approaches the room's ambient particle concentration. To measure and quantify the effectiveness of FFU clean air spread against the room's ambient particle concentration, the following empirical formula is used to

describe the spread of clean air protection in relation to the axial dimensionless distance in expression (4):

$$\frac{c_e - c_m(x)}{c_e - c_0} = A \left(\frac{x}{R_0} \right)^B \quad (4)$$

where c_e is the particulate concentration in the surrounding ambient environment and $c_m(x)$ is particulate concentration variable along the axial distance in Figure 1. c_0 is the particulate concentration in the supply air, and it is close to zero because a H14 HEPA filter is used in the FFU. "A" and "B" are the coefficient and exponent, respectively, which are to be numerically determined using regression based on the experimental data, as shown in expressions (5) and (6), which are correlated to the supply air face velocity.

$$A = 1.005(u_0)^{-0.863} \quad (5)$$

$$B = -0.1692(u_0)^{-1.461} \quad (6)$$

The left side of expression (4) is the axial dimensionless particulate concentration (abbreviated as ADPC), which reflects the deviation between particulate concentration $c_m(x)$ and the surrounding environment particulate concentration c_e . Based on this definition, the ADPC value ranges from 1 to 0, which, respectively, represents a plane where clean air starts at the FFU discharge and ends at the final contour where the clean airstream gradually loses its impact and its concentration approaches the concentration of the surrounding room air.

Figure 6 shows the variation in the ADPC along the axial direction with various supply air velocities. The magnitude of the ADPC is almost inversely proportional to the axial distance from the FFU, and air is cleaner with the increase in the supply air face velocity. The test results show that ADPC is affected by both distance and face velocity from the FFU. For example, at the same location of $x/R_0 = 6.842$, the ADPC value increases from 0.425 to 0.825 when the face velocity u_0 increases from 0.281 m/s (Case 1) to 0.716 m/s (Case 4).

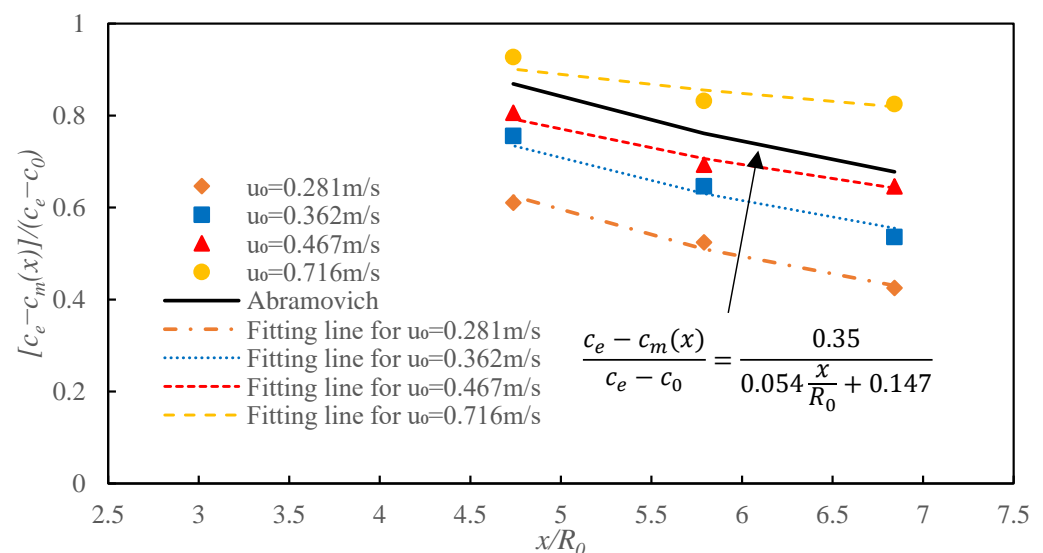


Figure 6. Dimensionless concentration along the axial direction under various face velocities.

Abramovich [19] studied the diffusion distribution of pollutants discharged into a clean environment from a circle nozzle jet along the axial direction and obtained an empirical expression, as shown in Figure 6. The results were independent of the face velocity. Abramovich's curve follows a similar trend as the calculated curves for the four experimental face velocities.

At a specific axial position, a higher ADPC value means a cleaner air stream against the surrounding contaminated room air. However, clean supply air loses its cleaning and dilution capability after continuous velocity decay along the axial direction. If a working height is 0.8~1.2 m from the floor (0.9~1.3 m from the FFU in this study), based on expression (4), the ADPC value decreases by 21~34% when the FFU face velocity increases by 10%.

3.5. Spread of Clean Air from the FFU along the Lateral Direction

The measured particulate concentration $c(x,y)/c_e$ at three cross-section heights ($x = 0.9$ m, $x = 1.1$ m, and $x = 1.3$ m) with four supply air face velocities are shown in Figure 7, where $c(x,y)$ denotes the local particulate concentration at a lateral distance y from the centerline of the FFU. As shown in the figure, the particulate concentration increases (air cleanliness decreases) with the increase in lateral distance y/R_0 and with the increase in axial distance x/R_0 . Charts a/b/c in Figure 7 also confirm a typical jet air behavior where the particle concentration under the FFU airstream approaches the ambient concentration faster at a higher elevation ($x = 0.9$ m) than those at lower elevations ($x = 1.1$ m and 1.3 m).

Clean supply air, with almost zero particle concentration, starts spreading from the FFU discharge and ends where the clean air mixed airstream concentration gradually approaches the concentration in the surrounding room air. The clean air from the starting to the ending borders forms a cone-shaped clean air protection region. The lateral distance y/R_0 when $c(x,y)/c_e = 1$ is the maximum impact range that the clean air jet can influence. Figure 7 shows that the lateral impact range becomes wider along the downward axial direction and that a higher face velocity can enlarge the clean air protection region.

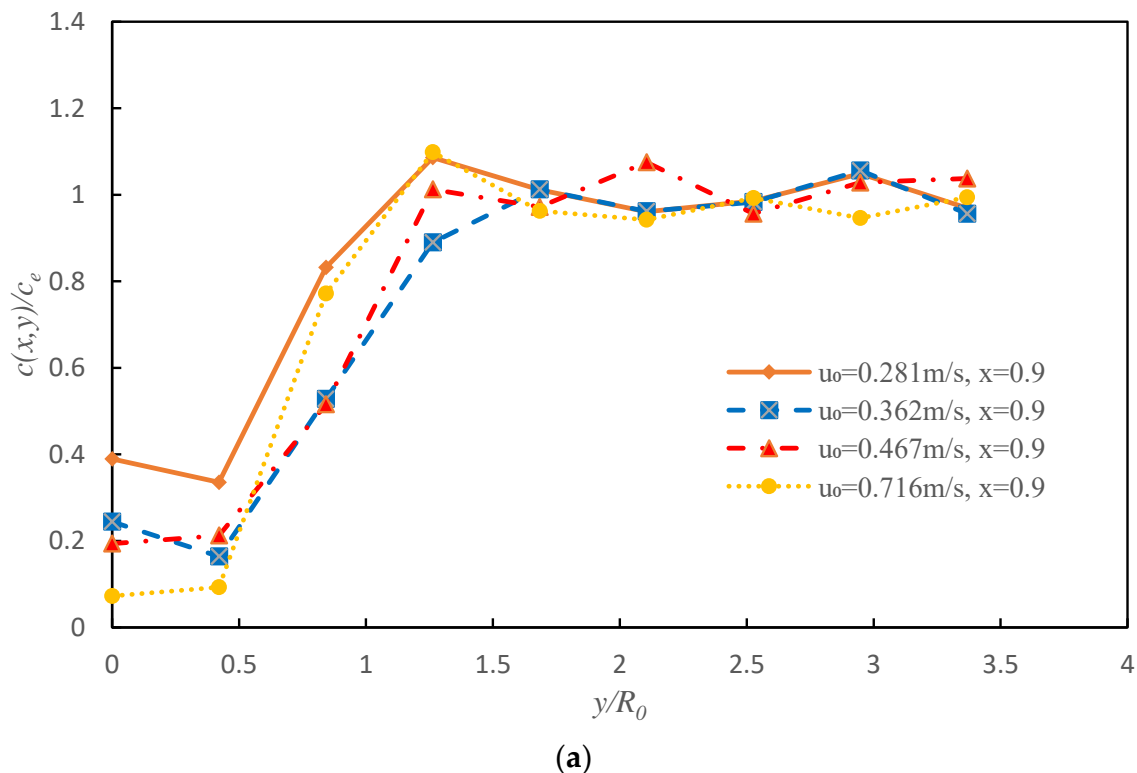


Figure 7. Cont.

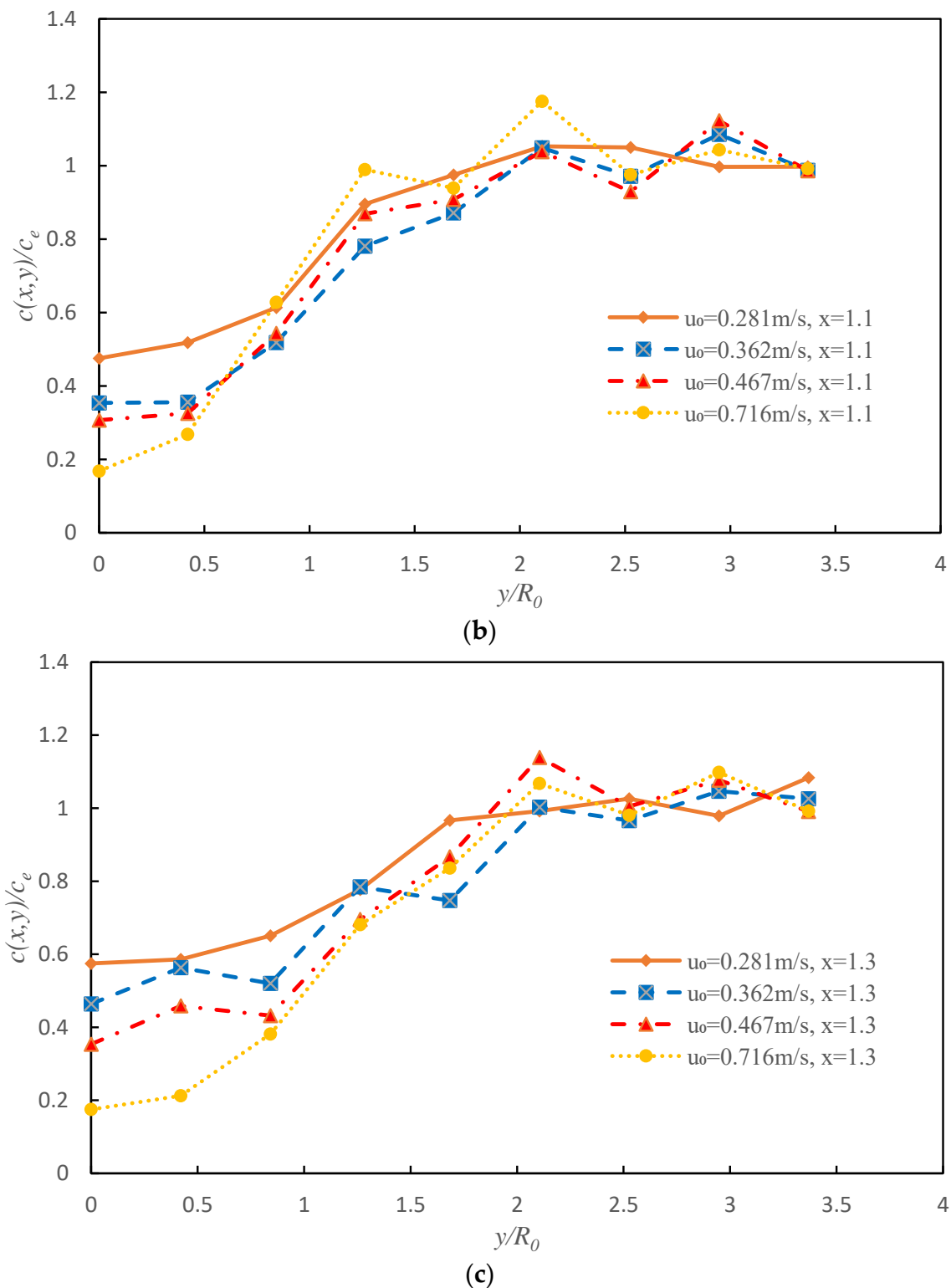


Figure 7. Clean air-impacted particulate concentration along a lateral direction at various elevations. (a) $x = 0.9$ m section, $x/R_0 = 4.74$; (b) $x = 1.1$ m section, $x/R_0 = 5.79$; and (c) $x = 1.3$ m section, $x/R_0 = 6.84$.

Abramovich [19] obtained expression (7) to calculate a pollutant concentration $[c_e - c(x,y)] / (c_e - c_m)$ with dimensionless radial distance y/y_{ce} , for a scenario in which an air jet containing pollutants is injected into a clean air environment, where y_{ce} represents the distance y where the pollutant concentration $c(x, y)$ reaches zero as the room's concentration. On the

contrary in this study, clean air is injected into the polluted room environment. Inspired by Abramovich’s expression, the authors of this study used a similar empirical structure but redefined y_{ce} as the distance y where the particulate concentration in clean airstream rises and reaches the ambient room concentration c_e . The values calculated using redefined expression (7) are compared to the experimental data with various supply air velocities in Figure 8. The results show that the curve of Abramovich’s redefined expression corresponds well to the experimental data in the lateral direction. Table 5 lists the MAPE values, with a range of 11.8~18.6%, between the calculated results of redefined expression (7) and the experimental results for four supply air velocities.

$$\frac{c_e - c(x, y)}{c_e - c_m(x)} = 1 - \left(\frac{y}{y_{ce}}\right)^{1.5} \tag{7}$$

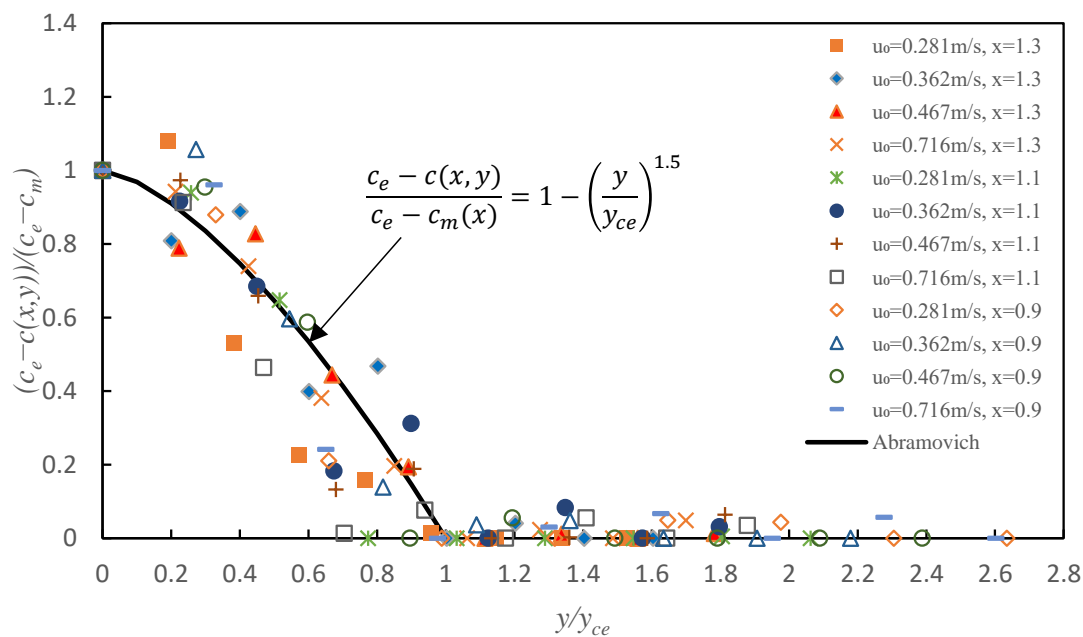


Figure 8. Particulate concentration along the lateral direction (normalized and dimensionless) under various face velocities and elevations.

Table 5. MAPE between experimental data and values calculated using Abramovich’s expression.

Test Case	$u_0 = 0.281$ m/s	$u_0 = 0.362$ m/s	$u_0 = 0.467$ m/s	$u_0 = 0.716$ m/s
MAPE	17.3%	18.6%	11.8%	13.6%

3.6. Width of the Clean Air Diffusion Boundary

Expression (8) uses a linear relationship between the width of clean air diffusion y_{ce}/R_0 and the axial distances x/R_0 , where the constants are obtained using curve fitting. Figure 9 depicts the experimental results, and the MAPE values are listed in Table 6. The impact of various discharge velocities u_0 seems limited. These observations indicate that the clean air boundary (measured as diffusion width) is almost in a straight-angle cone shape at a fixed slope.

$$\frac{y_{ce}}{R_0} = 0.1788 \frac{x}{R_0} + 0.6776 \tag{8}$$

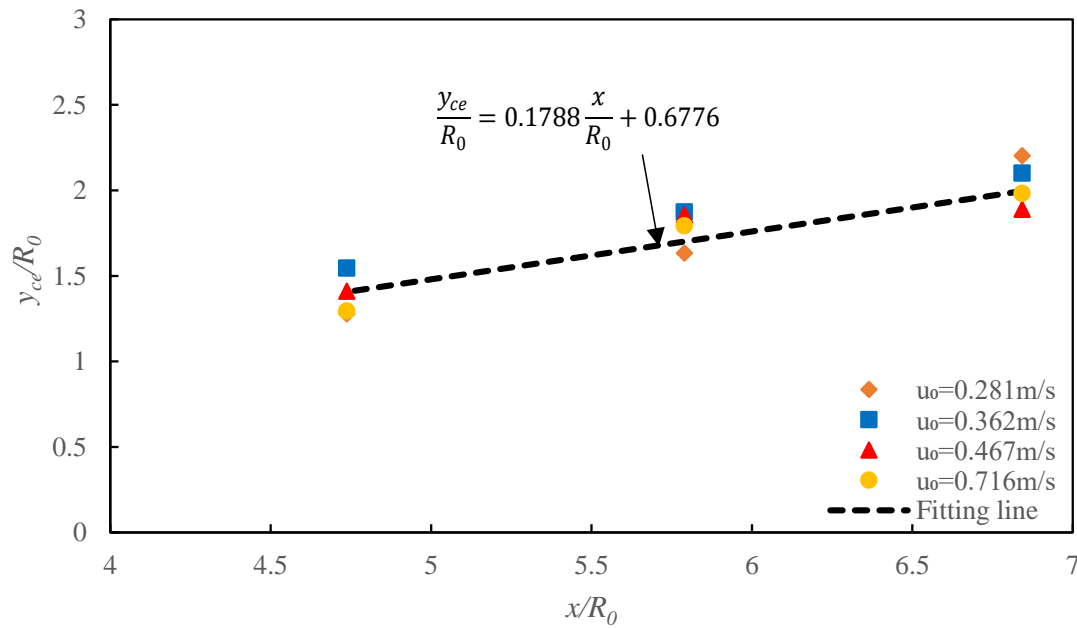


Figure 9. The width of clean air diffusion y_{ce}/R_0 is almost linear with axial distance x/R_0 .

Table 6. MAPE between the fitting expression and experimental value.

Test Case	$u_0 = 0.281 \text{ m/s}$	$u_0 = 0.362 \text{ m/s}$	$u_0 = 0.467 \text{ m/s}$	$u_0 = 0.716 \text{ m/s}$
MAPE	12.6%	6.5%	5.5%	8.8%

4. Calculation Models for FFU Airflow Diffusion and Clean Air Spread

By combining expression (1) and expression (2), the dimensionless velocity at any position downstream of the FFU can be expressed as follows:

$$\frac{u(x, y)}{u_0} = \frac{u_m(x)}{u_0} \times \frac{u(x, y)}{u_m(x)} = 1.422 \left(\frac{x}{R_0} \right)^{-0.338} \times \left(-0.1472\eta^4 + 0.7714\eta^3 - 1.2003\eta^2 + 0.0925\eta + 1 \right) \quad (9)$$

Substituting expression (3) of dimensionless lateral distance $\eta = y/y_{0.5um}$ into expression (9), expression (10) is obtained. It can be observed that the velocity $u(x, y)$ at any position is related to the supply air face velocity u_0 , the size R_0 of the FFU, the axial distance x from the FFU, and the radial distance y from the centerline of the FFU.

$$\frac{u(x, y)}{u_0} = 1.422 \left(\frac{x}{R_0} \right)^{-0.338} \times \left[-0.1472 \left(\frac{y}{0.0961x + 0.428R_0} \right)^4 + 0.7714 \left(\frac{y}{0.0961x + 0.428R_0} \right)^3 - 1.2003 \left(\frac{y}{0.0961x + 0.428R_0} \right)^2 + 0.0925 \left(\frac{y}{0.0961x + 0.428R_0} \right) + 1 \right] \quad (10)$$

Similarly, using mathematical operations among expression (4), expression (7), and expression (8), the dimensionless particulate concentration $c(x, y)/c_e$ (as the measure of air cleanliness level) at any position downstream of the FFU can be obtained with expression (11). Expression (11) is related to the room ambient particulate concentration c_e , the supply air particulate concentration c_0 , and the size R_0 of the FFU, in addition to the distance variables x and y .

$$\frac{c_e - c(x, y)}{c_e - c_0} = A \left(\frac{x}{R_0} \right)^B \times \left[1 - \left(\frac{y}{0.1788x + 0.6776R_0} \right)^{1.5} \right] \quad (11)$$

As HEPA media ($\geq 99.97\%$ efficiency) are typically installed inside an FFU, the supply air concentration c_0 is approximately zero. Expression (11) can be simplified into expres-

sion (12), where the coefficient A and exponent B are obtained using expression (5) and expression (6) with numerical fitting.

$$\frac{c(x, y)}{c_e} = 1 - A \left(\frac{x}{R_0} \right)^B \times \left[1 - \left(\frac{y}{0.1788x + 0.6776R_0} \right)^{1.5} \right] \quad (12)$$

Experimental tests were conducted under four face velocities ($u_0 = 0.281$ m/s, 0.362 m/s, 0.467 m/s, and 0.716 m/s) and at three elevations ($x = 1.3$ m, 1.1 m, and 0.9 m) to validate the accuracy of the new calculation models of expressions (10) and (12). The resulting MAPE values are listed in Table 7. It is found that the mean error in the particulate concentration predictions is in the range of 8.6~15.2%, and the error in the air velocity predictions is between 10.3% and 13.2%. These new models can be utilized to estimate both the air velocity and particle concentration (as the measure of air cleanliness level) in any position under the FFU flow region with acceptable accuracies.

Table 7. MAPE of the calculated model.

Test Case	$u_0 = 0.281$ m/s	$u_0 = 0.362$ m/s	$u_0 = 0.467$ m/s	$u_0 = 0.716$ m/s
Air velocity ($\eta \leq 2$)	-	13.2%	10.3%	11.3%
Particulate concentration	8.6%	11.9%	11.0%	15.2%

5. Integrated Effects of the FFU Outlet Size and Face Velocity on Clean Air Distribution

The new empirical models indicate that the air velocity and particulate concentration at any position downstream of the FFU are affected by the FFU face velocity u_0 and size R_0 . The following calculation conditions are used to compare and analyze the distributions of air velocity and particle concentration based on the new models, as outlined below: 2.7 m for room height; 0.61 m \times 0.61 m, 0.50 m \times 0.50 m, and 0.38 m \times 0.38 m for the three FFU face sizes, respectively; and 0.35 m/s, 0.40 m/s, and 0.45 m/s for the three FFU supply air face velocities, respectively. The common cleanroom workspace height is around 0.8~1.5 m from the floor; thus, the distance between the supply air outlet and the workspace x is 1.9~1.2 m.

In order to quantify the influenced range of supply airflow on the downstream velocity distribution, the radial distance y where the velocity is 10% of the face velocity u_0 is defined as the velocity diffusion boundary $y_{0.1u_0}$, which can be calculated for any point along lateral direction using expression (10).

Similarly, the influenced range of supply airflow on the downstream clean air diffusion (expansion with dilution to the room's air concentration) can also be obtained. The clean air diffusion boundary $y_{0.9c_e}$ is defined where the downstream ambient particulate concentration at cross-section reaches 90% of the ambient particulate concentration c_e , which can be derived from the expression (12) into the expression (13)

$$y_{0.9c_e} = (0.1788x + 0.6776R_0) \times \left\{ 1 - 0.1 \frac{1}{A} \left(\frac{x}{R_0} \right)^{-B} \right\}^{2/3} \quad (13)$$

Using the same method, the half protection range $y_{0.5c_e}$ can be defined, which is the radial distance y where the downstream particulate concentration is 50% of the ambient particulate concentration c_e in expression (14).

$$y_{0.5c_e} = (0.1788x + 0.6776R_0) \times \left\{ 1 - 0.5 \frac{1}{A} \left(\frac{x}{R_0} \right)^{-B} \right\}^{2/3} \quad (14)$$

5.1. Velocity and Particulate Concentration Distribution Using the New Models

The curves in Figure 10 are calculated using the new calculation models of expressions (10) and (12) with various FFU face velocities and sizes at the axial distance x of 1.2 m and

1.9 m, respectively. It can be found that the influence range increase significantly with the air outlet and with the air velocity. In addition, the distance from the supply air outlet has a significant effect. The further away from the supply air outlet, the smoother the air velocity curve.

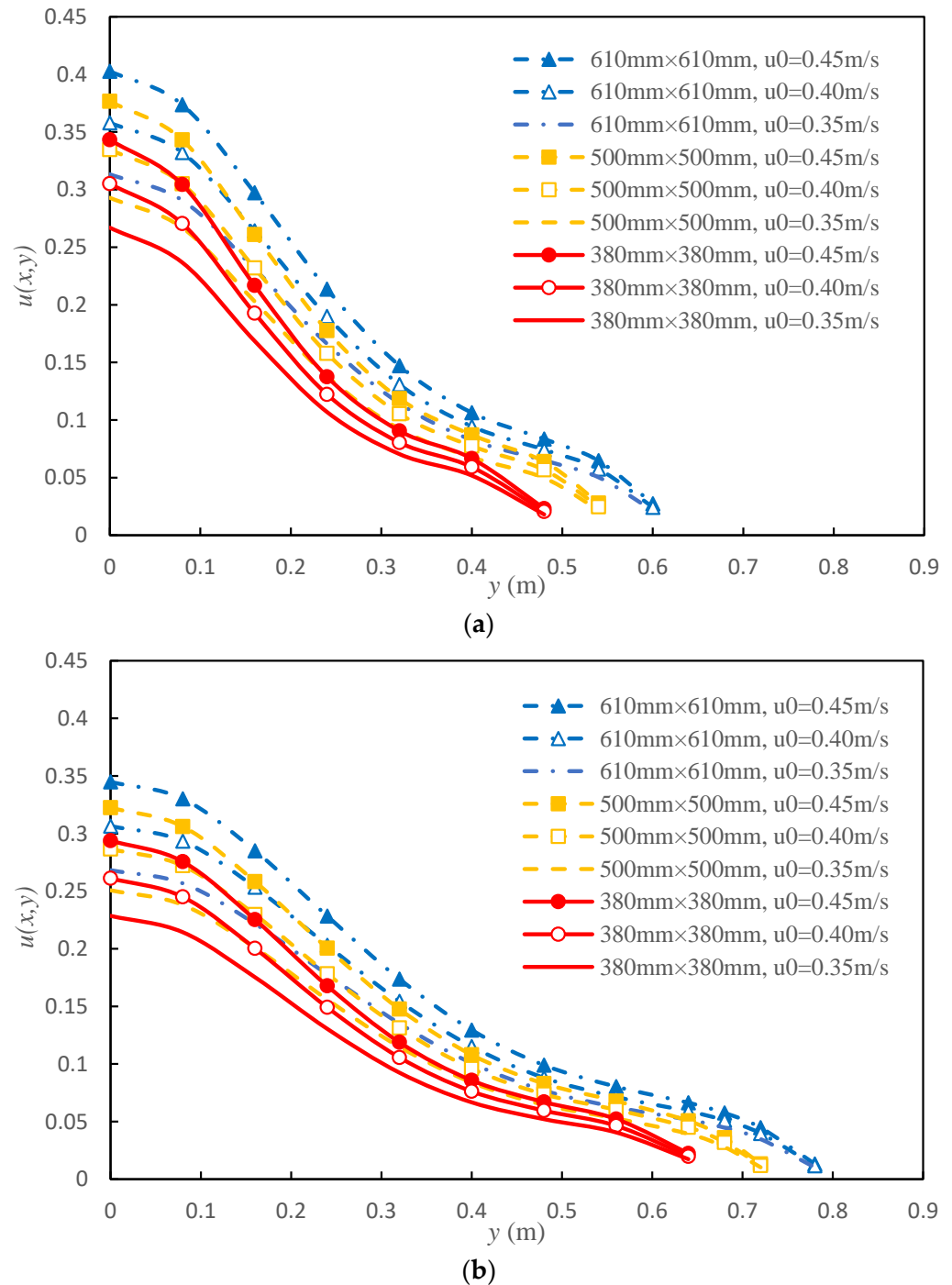


Figure 10. Air velocity distribution along the lateral direction at three elevations under various combinations of FFU face velocities and outlet sizes: (a) $x = 1.2$ m (1.5 m from the floor) and (b) $x = 1.9$ m (0.8 m from the floor).

Figure 11 shows the calculated particulate concentration distribution along the axial direction. The new model can be used to analyze the benefit of a larger FFU face size. As an example, for the same air face velocity u_0 of 0.4 m/s, if the FFU size is increased from

0.38 m × 0.38 m to 0.61 m × 0.61 m, the 257.7% size increment will lead to a reduction in the dimensionless particulate concentration $c(x,y)/c_e$ of about 74.1% and 34.9% at the axial distance x from 1.2 m to 1.9 m along the FFU centerline, respectively, and an expansion in the clean air diffusion boundary $y_{0.9ce}$ by 26.4% and 21.7%, respectively.

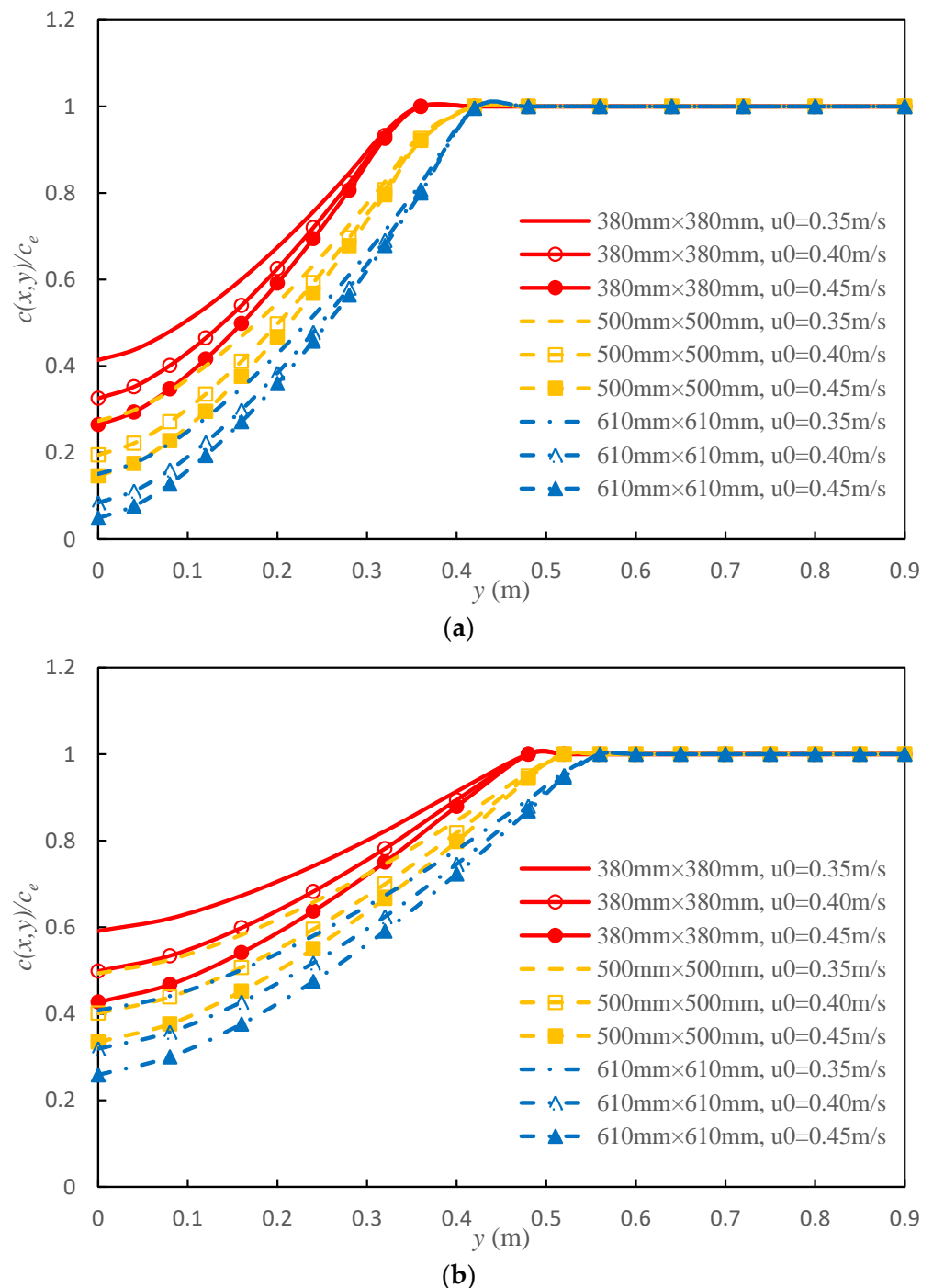


Figure 11. Dimensionless particulate concentration along the lateral direction at two elevations under various combinations of FFU face velocities and outlet sizes: (a) $x = 1.2$ m (1.5 m from the floor) and (b) $x = 1.9$ m (0.8 m from the floor).

5.2. Boundaries of Clean Air Diffusion and the Cleanliness Protection Region

Compared with the calculated values for the velocity and particulate concentration distributions in Figures 10 and 11, respectively, an interesting phenomenon is observed: The

impact of face velocity on the downstream velocity diffusion range is greater than that on the clean air's cleanliness diffusion range, which means that the diffusion ranges of velocity and cleanliness protection are not identical in width under the same conditions. Figure 12 shows an example of the diffusion widths of air velocity and cleanliness protection for three FFU face sizes under a discharge velocity of 0.4 m/s. Although a different percentage value could be assigned to define the width of the velocity diffusion boundary and the width of the clean air protection boundary, in Figure 12, the velocity diffusion boundary of $y_{0.1u0}$ and clean air protection boundary of $y_{0.5ce}$ and $y_{0.9ce}$ are used for an exemplary graphical illustration. Obviously, $y_{0.1u0}$ is larger than $y_{0.9ce}$. In commercial spaces, the local air particle concentration is not as critical as the local air velocity, which is related to the occupants' comfort; however, occupants in cleanrooms wear gowns and headcovers and typically receive a much higher ventilation rate per person, and the air cleanliness class is more critical to achieving process/manufacturing specifications. The experimental and calculated results show that in terms of the sensitivity of local air cleanliness to the FFU supply air (of various face sizes and velocities), it is more effective to use the cleanliness protection range boundary than the air velocity diffusion boundary in order to properly evaluate the particulate concentration distribution and its variations under the FFU airstream. In Figure 12, the curve for $y_{0.5ce}$ is completely different from that for $y_{0.9ce}$, which increases slightly at first and then decreases gradually with the axial direction. On the other hand, with an increase in the size of the supply air outlet, $y_{0.5ce}$ obviously increases, which implies that the larger supply air outlet has a larger cleanliness protection range.

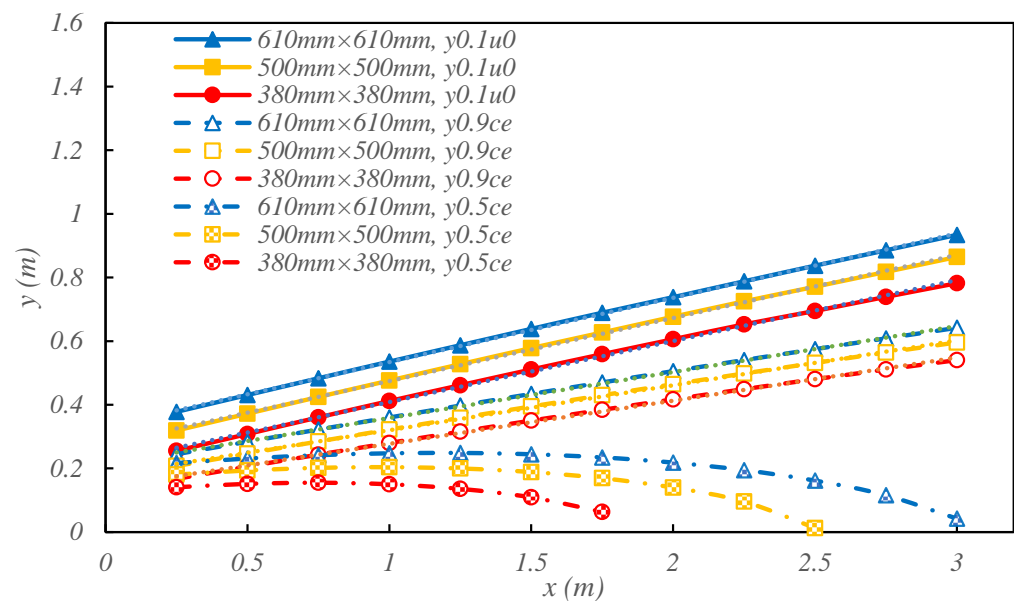


Figure 12. Example showing the clean air velocity diffusion boundary width and cleanliness protection boundary width ($u_0 = 0.4$ m/s).

5.3. Methodology to Calculate the Required FFU Supply Volume for a Required Downstream Air Cleanliness Level with Known FFU Face Sizes

The supply air volume is the key factor affecting the fan energy consumption of cleanrooms. It is necessary to investigate the required supply air volume with various sizes of supply air outlets to achieve the same cleanliness. In the calculation, we first determine the ratio c_e/c_0 . The air velocity required for various sizes of air outlets can be calculated using the expression (12), and then the supply air volume can be obtained. It was indicated earlier in this paper that the particulate concentration downstream of the FFU varies greatly with the axial distance. Considering the range of the workspace, the $x = 1.9$ m section (0.8 m from the floor) is selected for analysis. To illustrate the calculation methodology, Figure 13

shows the supply air volume for three FFU face sizes that are required to achieve the same particulate concentration along the FFU axial centerline position at this sectional height.

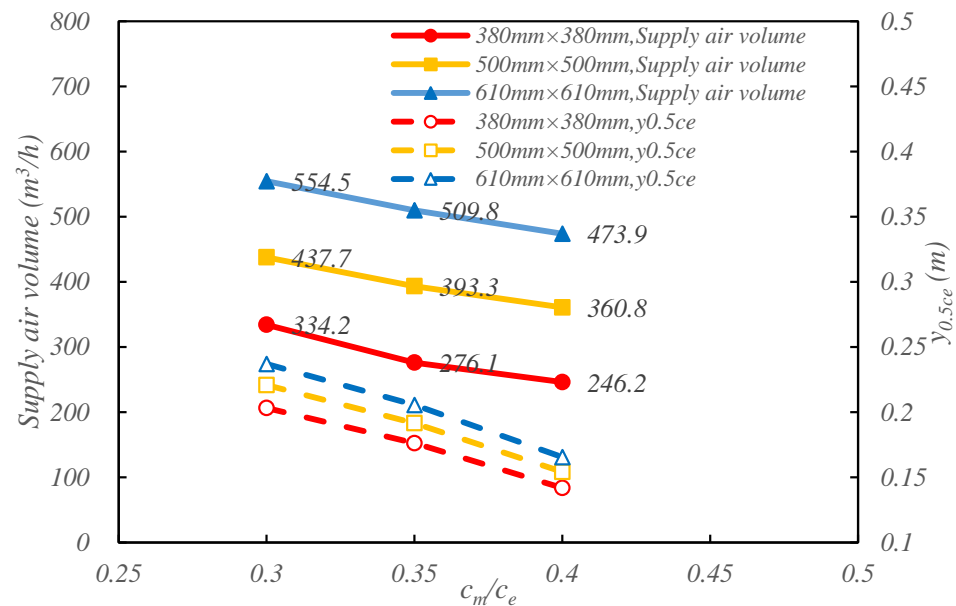


Figure 13. Example showing the required FFU supply volume for the required air cleanliness (30–40% of ambient concentration) along the centerline of several FFU outlet sizes ($x = 1.9$ m).

Figure 13 also plots the variation curve for $y_{0.5ce}$, which represents the decrease in the half-width protection range with the increase in particulate concentration at the axis position. It is found that the required air volume for the three supply air outlet sizes is $334.2 \text{ m}^3/\text{h}$, $437.7 \text{ m}^3/\text{h}$, and $554.5 \text{ m}^3/\text{h}$, respectively, when the particulate concentration at the axis position is reduced to 30% of the ambient particulate concentration. Small-sized air outlets require less air volume and are more energy efficiency. On the other hand, the total protection width (two times the $y_{0.5ce}$) is 0.4 m, 0.44 m, and 0.48 m, respectively. Therefore, the size of the supply air outlet should be considered according to the size of the protected process in practical application.

This study has shown that when the process protection area size and its cleanliness requirements are known, the airflow and particulate concentration distribution in the protection region can be calculated using the proposed new models and unnecessary airflow oversupply can be avoided. Particulate concentration sensors can be strategically placed in the surrounding environment or protected areas to control the supply air volume based on the detected local concentrations. This requires that the rated supply air volume of the air conditioning system should exceed the calculated air volume so that when the working condition changes, the operating air volume can be adjusted accordingly.

6. Summary and Conclusions

In summary, the characteristics of FFU downstream air velocity and particle distribution with various supply air velocities and face sizes were studied using experiments and numerical analysis. New empirical models specifically suitable for cleanroom FFU applications were proposed. These new models used similar numerical structures as those used in old models, which were based on jet air expressions obtained from commercial space not from typical cleanroom settings, where the background air cleanliness (in ISO classes) levels should be well controlled to ultra-low particle concentration to avoid biased test results. In this study, the air velocity and particulate concentration along the axial and radial directions were typically expressed in dimensionless forms to prepare the results for better generality. The existing jet air expressions cover a narrower velocity range, while the new models were generated from a broader wider velocity range that is typical for

cleanrooms using FFU units as air supply outlets. The integrated (coupling) effects of various FFU outlet sizes and supply air face velocities were further explored.

Below are the key conclusions:

- (1) The air distribution provided by various supply air velocities is similar. Along the axial direction, the downstream air velocity of the FFU gradually attenuates with the increase in axial distance. The increase in supply air face velocity can decrease the downstream particle concentration significantly. When the supply air face velocity was increased by 10%, the particle concentration along the axial direction was reduced by about 21~34%. Since the FFU air velocity (less than 1 m/s) is generally much lower than the velocity range suitable for traditional jet empirical expression, there was a noticeable gap between the measured value and the predicted value using the existing empirical expression. At cross-sections downstream of the FFU, the influence of FFU velocity progressively weakened with the increase in lateral distance, and the particle concentration gradually approached the surrounding ambient concentration. The airstream velocity and particle concentration were close to the predicted values using the existing jet air expressions.
- (2) Using the established new calculation models, the supply air volume that satisfies cleanliness requirements was studied under different supply outlet sizes and velocities. This paper used the common definitions of airflow velocity diffusion boundary (lateral distance when the axial velocity reaches 50% of the FFU face velocity) and air cleanliness protection range boundary (lateral distance when the particulate concentration under the FFU reaches or exceeds 50% of the ambient particulate concentration). For the axial position at 0.8 m from the floor, if the particle concentration needs to be reduced to 30% of the surrounding ambient concentration, the three sizes of supply air outlets (0.38 m × 0.38 m, 0.5 m × 0.5 m, and 0.61 m × 0.61 m) required the respective airflow volumes of 334.2 m³/h, 437.7 m³/h, and 554.5 m³/h. In addition, the total width of their protection range increased from 0.4 m, 0.44 m, to 0.48 m, respectively.
- (3) In order to properly evaluate the particle concentration distribution and its variations under the FFU airstream, it is more effective to use the cleanliness protection range boundary than the air velocity diffusion boundary.

The size of the supply air outlet and the supply air face velocity have significant effects on the particulate concentration distribution in the airflow range from the supply air outlet. A reasonable design of the supply air outlet size and supply air face velocity is necessary for cleanroom energy saving. The new calculation models and results of velocity distribution and clean air protection with various supply air velocities and sizes of supply air outlet given in this paper can provide a valuable reference for the future design of cleanroom air-conditioning systems. The results can also be used to update CFD algorithms specifically for cleanroom applications where FFUs are used as supply air outlets.

Author Contributions: Conceptualization, H.L.; Methodology, H.L.; Investigation, W.Y. and C.L.; Writing—original draft, H.L.; Writing—review & editing, C.H. All authors have read and agreed to the published version of the manuscript.

Funding: This work was supported by the Shanghai Natural Science Foundation (21ZR1444800).

Institutional Review Board Statement: Not applicable.

Informed Consent Statement: Not applicable.

Data Availability Statement: The data that support the findings of this study are available on request from the corresponding author.

Conflicts of Interest: The authors declare no conflict of interest.

Nomenclature

A	coefficient in expression (4)
B	exponent in expression (4)
$c(x,y)$	local particulate concentration at a lateral distance y from the centerline of an FFU
c_0	air particulate concentration in the FFU discharge air
c_e	particulate concentration in the surrounding environment
$c_m(x)$	particulate concentration variable along axial distance
R_0	half width of the FFU face surface
$u(x,y)$	local velocity at an axial/centerline distance x downstream of the FFU and a lateral distance y from the FFU centerline
u_0	FFU face velocity
$u_m(x)$	local velocity at the vertical distance x from the FFU
x	axial (vertical) distance from the FFU
y	radial (horizontal) distance at the cross-section from the vertical axis
$y_{0.1u_0}$	radial distance y where the velocity is 10% of the face velocity u_0 is defined as $y_{0.1u_0}$
$y_{0.5c_e}$	half protection range, the radial distance y where the downstream particulate concentration is 50% of the ambient particulate concentration c_e
$y_{0.5u_m}$	lateral distance y where the velocity is 50% of u_m
$y_{0.9c_e}$	lateral distance y where downstream particulate concentration at the cross-section reaches 90% of the ambient particulate concentration c_e
y_{c_e}	lateral distance y where the particulate concentration is equal to the ambient particulate concentration c_e
η	dimensionless lateral distance $y/y_{0.5u_m}$

References

- Naughton, P. History of Cleanrooms. *ASHRAE J.* **2019**, *61*, 38–54. Available online: www.ashrae.org (accessed on 17 September 2021).
- Whyte, W. *Cleanroom Technology*; John Wiley & Sons, Ltd.: Chichester, UK, 2001. [[CrossRef](#)]
- Kircher, K.; Shi, X.; Patil, S.; Zhang, K.M. Cleanroom energy efficiency strategies: Modeling and simulation. *Energy Build.* **2010**, *42*, 282–289. [[CrossRef](#)]
- Liu, J.; Zhang, L.; Yang, J.; Chen, Y.; Zhang, X. Study on pressure control and energy saving of cleanroom in purification air conditioning system. *Energy Build.* **2021**, *253*, 111502. [[CrossRef](#)]
- Ma, Z.; Liu, X.; Zhang, T. Measurement and optimization on the energy consumption of fans in semiconductor cleanrooms. *Build. Environ.* **2021**, *197*, 107842. [[CrossRef](#)]
- Fedotov, A. Saving energy in cleanrooms. *Cleanroom Technol.* **2014**, *22*, 14–18.
- Whyte, W.; Lenegan, N.; Eaton, T. Calculation of airborne cleanliness and air supply rate for non-unidirectional airflow cleanrooms. *Eur. J. Parenter. Pharm. Sci.* **2016**, *21*, 79–88.
- Zhou, L.; Sun, W.; Wu, C.; Li, H.; Zou, Z.; Huang, C. General particle concentration model and experimental validation for cleanrooms. *Sādhanā* **2020**, *45*, 198. [[CrossRef](#)]
- Sun, W.; Mitchell, J.; Flyzik, K.; Hu, S.C.; Liu, J.; Vijayakumar, R.; Fukuda, H. Development of cleanroom required airflow rate model based on establishment of theoretical basis and lab validation. *ASHRAE Trans. Am. Soc. Heat. Refrig. Air-Cond. Eng. (ASHRAE)* **2010**, *116*, 87–97.
- Whyte, W.; Whyte, W.; Eaton, T.; Lenegan, N. Calculation of air supply rates for nonunidirectional airflow cleanrooms. *Eur. J. Parenter. Pharm. Sci.* **2014**, *19*, 121–129.
- Whyte, W.; Lenegan, N.; Eaton, T. Equations for predicting airborne cleanliness in non-unidirectional airflow cleanrooms. *Eur. J. Parenter. Pharm. Sci.* **2016**, *21*, 38–43.
- Goldstein, K.; Divelbiss, J. Design of Cleanroom Airflows for Particle Control Using CFD Analysis: Case Studies. In *Particles in Gases and Liquids 3*; Springer: Boston, MA, USA, 1993; pp. 171–187. [[CrossRef](#)]
- Whyte, W.; Hejab, M.; Whyte, W.M.; Green, G. Experimental and CFD airflow studies of a cleanroom with special respect to air supply inlets. *Int. J. Vent.* **2010**, *9*, 197–209. [[CrossRef](#)]
- Loomans, M.G.L.C.; Molenaar, P.C.A.; Kort, H.S.M.; Joosten, P.H.J. Energy demand reduction in pharmaceutical cleanrooms through optimization of ventilation. *Energy Build.* **2019**, *202*, 109346. [[CrossRef](#)]
- Zhao, J.; Shao, X.; Li, X.; Liang, C.; Wang, H.; Xu, W. Theoretical expression for clean air volume in cleanrooms with non-uniform environments. *Build. Environ.* **2021**, *204*, 108168. [[CrossRef](#)]
- ISO 14644-16; Cleanrooms and Associated Controlled Environments—Part 16: Energy Efficiency in Cleanrooms and Separative Devices. ISO: Geneva, Switzerland, 2019.
- Ma, R.H. Study on simulation of airflow within the enclosure in the semiconductor factory cleanroom. *Aerosol Sci. Technol.* **2006**, *40*, 282–292. [[CrossRef](#)]
- Eslami, J.; Abbassi, A.; Saidi, M.H.; Bahrami, M. Effect of supply/exhaust diffuser configurations on the contaminant distribution in ultra clean environments: Eulerian and Lagrangian approaches. *Energy Build.* **2016**, *127*, 648–657. [[CrossRef](#)]
- Abramovich, G.N. *The Theory of Turbulent Jets*; The MIT Press: Cambridge, MA, USA, 2003. [[CrossRef](#)]

20. Rajaratnam, N. *Turbulent Jets*; Elsevier: Amsterdam, The Netherlands, 1976.
21. Zou, Y. Velocity decay in air jets for HVAC applications. *ASHRAE Trans.* **2000**, *106*, 53.
22. Ball, C.G.; Fellouah, H.; Pollard, A. The flow field in turbulent round free jets. *Prog. Aerosp. Sci.* **2012**, *50*, 1–26. [[CrossRef](#)]
23. Yao, S.; Guo, Y.; Jiang, N.; Liu, J. An experimental study of a turbulent jet impinging on a flat surface. *Int. J. Heat Mass Transf.* **2015**, *83*, 820–832. [[CrossRef](#)]
24. Dai, S.; Sun, H.; Liu, W.; Guo, Y.; Jiang, N.; Liu, J. Experimental study on characteristics of the jet flow from an aircraft gasper. *Build. Environ.* **2015**, *93*, 278–284. [[CrossRef](#)]
25. Standard, A. *ASHRAE Handbook Fundamentals 2017*; Ashrae: Peachtree Corners, GA, USA, 2017; pp. 20.2–20.8.
26. Yin, H.; Li, A.; Liu, Z.; Sun, Y.; Chen, T. Experimental study on airflow characteristics of a square column attached ventilation mode. *Build. Environ.* **2016**, *109*, 112–120. [[CrossRef](#)]
27. Yin, H. Study on Design Procedures of Air Distribution by Air Curtain Ventilation with a Linear Slot Diffuser. Ph.D. Thesis, Xi'an University of Architecture and Technology, Xi'an, China, 2013.
28. Laban, A.; Aleyasin, S.S.; Tachie, M.F.; Koupriyanov, M. Experimental investigation of nozzle spacing effects on characteristics of round twin free jets. *J. Fluids Eng. Trans. ASME* **2019**, *141*, 071201. [[CrossRef](#)]
29. Tollmien, W. Berechnung turbulenter Ausbreitungsvorgänge. *ZAMM—J. Appl. Math. Mech./Z. Für Angew. Math. Mech.* **1926**, *6*. [[CrossRef](#)]
30. Görtler, H. Berechnung von Aufgaben der freien Turbulenz auf Grund eines neuen Näherungsansatzes. *ZAMM—J. Appl. Math. Mech./Z. Für Angew. Math. Mech.* **1942**, *22*, 244–254. [[CrossRef](#)]

Disclaimer/Publisher's Note: The statements, opinions and data contained in all publications are solely those of the individual author(s) and contributor(s) and not of MDPI and/or the editor(s). MDPI and/or the editor(s) disclaim responsibility for any injury to people or property resulting from any ideas, methods, instructions or products referred to in the content.